Heliyon 10 (2024) e38951

Contents lists available at ScienceDirect

Heliyon

journal homepage: www.cell.com/heliyon

Research article

Proteomics-based network pharmacology and molecular docking reveal the potential mechanisms of 5,6,7,4′-tetramethoxyflavone against HeLa cancer cells

Qiang You [a,b,1], Lan Li [c,1], Haiyan Ding [d], Youping Liu [d,*]

[a] Department of Pharmacy, Hospital of Chengdu University of Traditional Chinese Medicine, Chengdu, 610072, China
[b] Department of Pharmacy, The Second Affiliated Hospital of Hainan Medical University, Haikou, Hainan, 570100, China
[c] School of Nursing, Peking University, Beijing, 100091, China
[d] School of Pharmacy, Chengdu University of Traditional Chinese Medicine, Chengdu, 611137, China

ARTICLE INFO

Keywords:
Polymethoxyflavones
5,6,7,4′-tetramethoxyflavone
Tetrametlglscutellarein
Proteomics
Mechanisms
Network pharmacology
Molecular docking
Cervical cancer
HeLa

ABSTRACT

Recent research has highlighted the therapeutic potential of citrus-derived dietary 5,6,7,4′-tetramethoxyflavone (TMF) against HeLa cancer. Our study aims to elucidate its mechanisms of action through proteomics analysis, network pharmacology, and molecular docking. The results suggested that TMF demonstrated efficacy by upregulating CD40, CD40L, Fas, Fas-L, HSP27, HSP60, IGFBP-1, IGFBP-2, IGF-1sR, Livin, p21, p27, sTNFR2, TRAILR2, TRAILAR3, TRAILR4, XIAP, p-Sre, p-Stat1, p-Stat2 p-c-Fos, p-SMAD1, p-SMAD2, p-SMAD4, p-SMAD5, p-IκBα, p-MSK1, p-NFκB, p-TAK1, p-TBK1, p-ZAP70, and p-MSK2, while downregulating p-EGFR, p-ATF2, p-cJUN, p-HSP27, p-JNK, and p-GSK3A. These targets are primarily involved in MAPK, apoptosis, and TNF signaling pathways. Notably, p21, p27, EGFR, SMAD4, JNK, ATF2, and c-JUN merged as pivotal targets contributing to TMF's anti-cancer efficacy against HeLa cells. This study is first to delineate the potential signaling pathways and core targets of TMF in treating of HeLa cancer, paving the way for further exploration of TMF's medical potential.

1. Introduction

Cervical cancer (CCA) ranks as the fourth most common malignancy among women globally, with approximately 604,000 new cases and 342,000 deaths reported in 2020 [1]. The vast majority of CCA cases are linked to persistent infections with high-risk human papillomavirus [2]. Due to the absence of organized screening and vaccination programs, developing countries account for nearly 90 % of the global burden of new cases and deaths [3]. Chemotherapy remains a cornerstone in the treatment of CCA, particularly in recurrent and advanced metastatic case, with cisplatin, gemcitabine, and paclitaxel commonly employed to improve patient prognosis

Abbreviations: BE, binding energy; BP, biological processes; CC, cellular components; CCA, cervical cancer; DEPs, differentially expressed proteins; DMSO, dimethyl sulfoxide; GO, gene ontology; KEGG, Kyoto encyclopedia of genes and genomes; MD, molecular dynamics; MF, molecular functions; PMF, polymethoxyflavones; PPI, protein-protein interaction; Rg, radius of gyration; RMSD, root mean squared deviation; RMSF, root mean square fluctuation; SASA, solvent accessible surface area; TMF, 5,6,7,4′-tetramethoxyflavone.

* Corresponding author. School of Pharmacy, Chengdu University of Traditional Chinese Medicine, 1166 Liutai Avenue, Wenjiang District, Chengdu 611137, China.
E-mail address: youpingliu@cdutcm.edu.cn (Y. Liu).

[1] These authors are co-first authors.

https://doi.org/10.1016/j.heliyon.2024.e38951
Received 17 June 2024; Received in revised form 23 August 2024; Accepted 3 October 2024
Available online 4 October 2024

and overall survival. However, the severe toxicities associated with these first-line chemotherapeutics, including neutropenia, vomiting, diarrhea, and even fatal outcomes, often undermine their clinical benefits [4]. Therefore, there is a critical need for research into effective CCA chemotherapeutics agents, with reduced toxicity.

Nature products have long been a significant source of anticancer agents [5]. An analysis of small-molecule antitumor drugs approved globally between the 1940s and 2011 worldwide revealed that approximately 50 % were natural products or their derivatives [6]. Among these, 5,6,7,4′-tetramethoxyflavone (TMF), a dietary polymethoxyflavone (PMF), is derived from various plant species, including *Citrus* species [7], *Nervilia concolor* [8], *Marrubium vulgare* [9], *Cissus assamica* [10] and *Clerodendranthus spicatus* [11], as well as the traditional Chinese herbal formula Gehua Jiecheng decoction [12]. Notably, TMF is abundantly found in the peel of citrus fruits, such as mandarin, orange, lemon and grapefruit. In different varieties of loose-skin mandarins, TMF content varies significantly, ranging from 0 to 13.7 mg/g, with the highest levels in 'Cupigoushigan' tangerine, while in sweet oranges, it generally ranges from 1 to 2 mg/g [7] (Fig. 1). TMF has been reported to possess broad-spectrum antitumor activity. For instance, Manthey et al. [13]isolated TMF from orange peel and found that it significantly inhibited the proliferation of various human cancer cell lines, including DMS-114, HT-29, MCF-7, DU-145, and MDA-MB-435. Subsequently, Ohtani et al. [14]demonstrated that TMF significantly enhanced the antitumor activity of vincristine in K562/ADM cancer cells by increasing vincristine uptake *via* P-glycoprotein inhibition. Additionally, TMF was shown to improve the inhibitory activity of 5-fluorouracil against HT29 colon cancer cells by upregulating CDH1 and downregulating ZEB1 and SNAI1 [15]. However, the current research on TMF's antitumor activity is largely confined to a limited number of *in vitro* studies. One of the main challenges has been the lower concentration of TMF compared to other well-studied PMFs, such as nobiletin and tangeretin. Our previous research [16] synthesized 12 PMFs with high purity at gram scale through the methylation of polyhydroxyflavones and assessed their pharmacokinetic parameters and antitumor activity against HeLa, A549, HepG2, and HCT116 cancer cells. Among these PMFs, only TMF significantly inhibited HeLa cells and was detectable in rat plasma, suggesting its potential as a promising therapeutic agent for CCA. Nevertheless, the underlying mechanisms of TMF's action against HeLa cancer remain unclear.

Antibody microarray, a cutting-edge proteomic profiling technology, allows for the rapid and simultaneous detection of multiple target protein expression levels. Compared to traditional western blotting, this technique offers advantages such as miniaturization, high throughput, enhanced sensitivity, and reduced sample requirement, making it a valuable tool in assessing tumor-related protein expression [17]. For instance, a previous study [18] utilized an antibody microarray to investigate the mechanisms behind baicalin-induced apoptosis in gastric cancer SGC-7901 cells. The study found that baicalin's apoptotic effect were primarily mediated through the upregulation of BAD, caspase-3, caspase-8, FasL, HSP60, TRAIL R4, IGF-I, IGF-II, P21, P27, p53, and SMAC, along with a marked downregulation of XIAP. These findings were subsequently confirmed by western blotting, which yielded results consistent with those of the antibody microarray.

This study aims to elucidate the molecular mechanisms underlying TMF's action against HeLa cancer by integrating proteomics analysis with network pharmacology and molecular docking approaches.

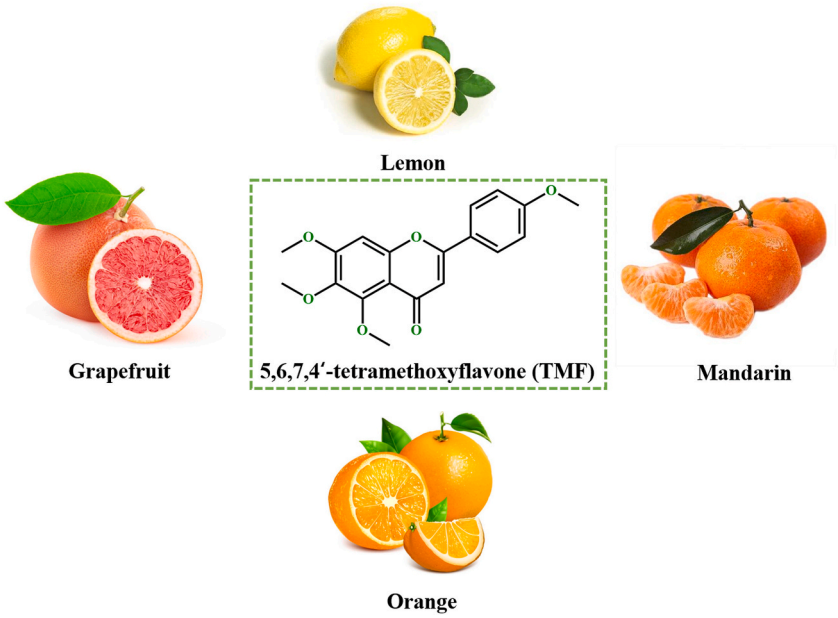

Fig. 1. The chemical structure of 5,6,7,4′-tetramethoxyflavone (TMF) and its primary sources.

2. Materials and method

2.1. Chemicals and reagents

The TMF (HPLC purity >98 %) used in this study was synthesized according to our previously published method [16]. Dimethyl sulfoxide (DMSO) (biochemical grade, BCCD7238) was obtained from Sigma-Aldrich (Shanghai) Trading Co., LTD. Fetal bovine serum (20200408) and trypsin-EDTA (70070200) solution were sourced from Biosharp (Beijing, China), while the penicillin-streptomycin (J190033) solution was procured from HyClone Laboratories (UT, USA).

2.2. Cell cultures and treatments

HeLa cells (ATCC Cat# CCL-2, RRID: CVCL_0300) were acquired from Chengdu University of Traditional Chinese Medicine. The cells were seeded in 5 mL of DMEM containing 10 % fetal bovine serum, penicillin (100 IU/mL), and streptomycin (100 μg/mL). Cultures were maintained in a humidified incubator at 37 °C with 5 % CO_2. TMF was dissolved in DMSO and prepared at a concentration of 50 mM. The cells were then passaged into six 60 mm Petri dishes at a density of 0.5×10^6 cells/well, with three dishes allocated to the experimental group and three to the control group. After 24 h of incubation, when the cell density reached a density of 1×10^6 cells/well, the experimental group was treated with 5 μL of TMF, resulting in a final concentration of 50 μM [16], while the control group received 5 μL of DMSO, yielding a final concentration of 0.1 % (v/v). Following an additional 24 h of incubation, the cells were washed twice with PBS and harvested into cryopreservation tubes.

2.3. Antibody array analysis

To explore the signaling pathways triggered by TMF, apoptosis-related proteins and phosphorylation sites were analyzed using the Human Phosphorylation Pathway Profiling Array C55 (Raybiotech, Inc., USA, AAP-PPP-1), encompassing 55 proteins, including EGFR (Ser1070), JAK1 (Tr1-22), JAK2 (Tyr1007/1008), SHP1 (Ser591), SHP2 (Tyr542), Src (Tyr419), Stat1 (Ser727), Stat2 (Tyr689), Stat3 (Tyr705), Stat5 (Tyr694), Stat6 (Tyr641), TYK2 (Tyr1054), ATF2 (T69/71), C-Fos (T232), c-JUN (S73), SMAD1 (S463/465), SMAD2 (S245/250/255), SMAD4 (T277), SMAD5 (S463/465), ATM (S1981), eIF2a (S51),HDAC2 (S394), HDAC4 (S632), IκBα (S32), MSK1 (S376), NFκB (S536), TAK1 (S412), TBK1 (S172), ZAP70(Y292), CREB (S133), ERK1 (T202/Y204)/ERK2 (Y185/Y187), HSP27 (S82), JNK (T183), MEK (S217/221), MKK3 (S189), MKK6 (S207), MSK2 (S360), p38 (T180/Y182), p53 (S15), RSK1 (S380), RSK2 (S382), AKT (S473), AMPKa (T172), BAD (S112), 4E-BP1 (T36),GSK3a (S21), GSK3b (S9), mTOR (S2448), P27 (T198), P70S6K (T421/S424), PDK1 (S241), PRAS40 (T246), PTEN (S380), RAF-1 (S301), and PRS6 (S235/236). Additionally, the Human Apoptosis Array C1 (Raybiotech, Inc., USA, AAP-APO-1) was used, covering 43 proteins, including BAD, BAX, BCL-2, BCL-w, BID, BIM, Caspase 3, Caspase 8, CD40, CD40 Ligand, cIAP-2, Cytochrome-C, DR6, Fas Ligand, HSP27, HSP60, HSP70, HTRA, IGF-1, IGF-2, IGFBP-1, IGFBP-2, IGFBP-3, IGFBP-4, IGFBP-5, IGFBP-6, IGF-1sR, Livin, p21, p27, p53, SMAC, Survivin, sTNFRI, sTNFR2, TNF-α, TNF-β, TRAIL R1, TRAIL R2, TRAIL R3, TRAIL R4, and XIAP.

The antibody experiment followed the kit's instructions meticulously. Total protein was extracted from HeLa cells using a cell lysis buffer, and protein concentrations were measured using a BCA Protein Assay Kit (Thermo Scientific, Pierce™ 23227). The antibody array membrane was placed in an incubator box, followed by addition of 2 mL of blocking buffer. After a 1-h incubation at room temperature, the blocking buffer was removed, and 350 μg of protein (2 mL) extracted from these HeLa cells was loaded onto the membrane. Following a 12-h incubation at 4 °C, the sample was removed, and the membrane was washed 3–4 times with 2 mL of Wash Buffer I-II for 5 min per wash. Subsequently, 1 mL of Biotin-Conjugated Anti-Cytokine was added and incubated at room temperature for 2 h, followed by another round of washing with Wash Buffer I-II. Lastly, 2 mL of HRP-Streptavidin Concentrate was applied. After completing these steps, Detection Buffer C/D (0.25/0.25 mL) was added, and protein visualization was performed using the Image-Quant LAS4000 Scanner (General Electric Company, USA). For significance analysis, fold change (*FC*) was used as the basic statistic. The formula $\mathrm{Ln}\ FC = |E - C|$ was used, where E represents the average expression level in the experimental group and C represents the control group. Differentially expressed proteins (DEPs) were identified with thresholds of $FC \geq 1.2$ [19].

2.4. Gene ontology (GO) functional annotation

GO analysis is a widely utilized system for gene function classification in biology, providing descriptions of gene products across three categories: biological processes (BP), cellular components (CC), and molecular functions (MF) [20]. In this study, GO functional annotation was applied to the 37 DEPs identified *via* antibody array analysis using the online DAVID database (https://david.ncifcrf.gov/). Terms were ranked and selected based on an adjusted p-value threshold of <0.05, with the p-value, DEP count, and enrichment factor serving as metrics to assess the significance and relevance of the enriched terms. Visualization of these terms were conducted using the free online platform Weishengxin (https://www.bioinformatics.com.cn [last accessed on 30 July 2022]).

2.5. Kyoto Encyclopedia of genes and Genomes (KEGG) pathway enrichment

For KEGG pathway enrichment analysis of the 37 DEPs, Fisher's exact test was employed through the data package clusterProfiler from R/Bioconductor, with *Homo sapiens* as the background reference. Pathway terms were selected if the number of DEPs enriched in a given pathway exceeded five and the p-value was less than 0.05, with subsequent visualization also performed *via* Weishengxin

(https://www.bioinformatics.com.cn [last accessed on 30 July 2022]).

2.6. Protein-protein interaction (PPI) analysis

To identify key DEPs, protein-protein interaction (PPI) analysis was conducted using the STRING online platform, version 11.5 (https://cn.string-db.org/), with the analysis restricted to Homo sapiens. The significance of DEPs within the network was determined by calculating the number of node connections using R software (version 3.6.0), reflecting their importance within the PPI network.

2.7. Molecular docking and molecular dynamics (MD) simulation

Molecular docking analysis was conducted to identify the binding sites and calculate the binding energy (BE) between TMF and the DEPs using AutoDock Vina 1.1.2. The 2D and 3D chemical structures of TMF were created with ChemDraw Professional 19.0. Before

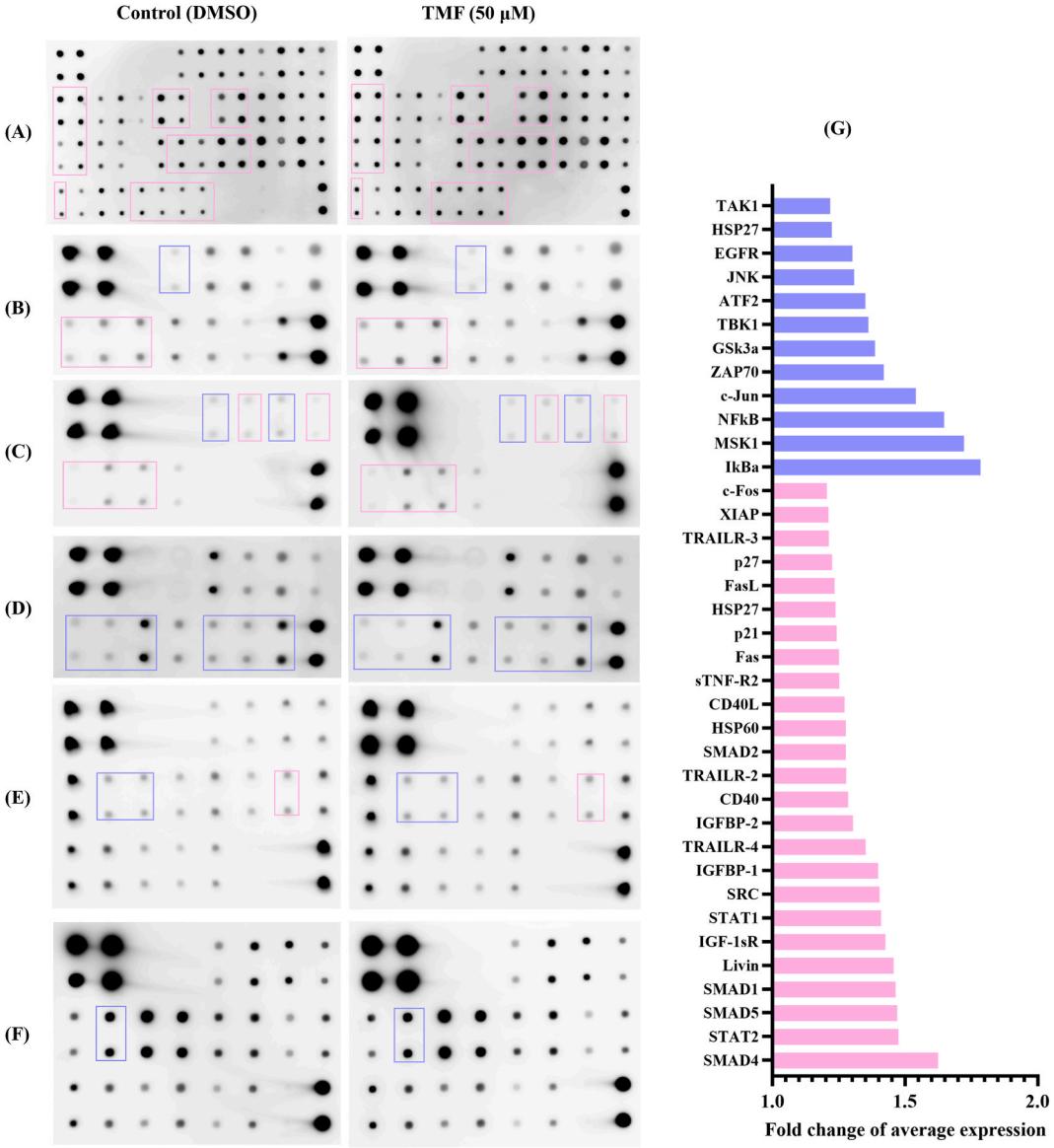

Fig. 2. Effects of TMF on the proteome of HeLa cells using Human cytokine antibody microarray analysis. (A) Apoptosis-associated antibody array, (B) JAK/STAT signaling pathway array, (C) TGF-β signaling pathway array, (D) NFκB signaling pathway array, (E) MAPK signaling pathway array, (F) AKT signaling pathway array, and (G) Graphic representation of the 37 differentially expressed proteins (DEPs) in HeLa cells treated with TMF (50 μM) (FC > 1.2). Among the 37 DEPs, 12 were downregulated, and 25 were upregulated. Note: Red columns and frames indicate significant upregulation, while blue columns and frames indicate significant downregulation.

performing the docking analysis, the 3D structure of TMF was optimized using MM2 minimization. The 3D structures of the DEPs were obtained from the Protein Data Bank (PDB) (https://www.rcsb.org/) and the AlphaFold Protein Structure Database (https://alphafold.ebi.ac.uk/). BE serves as an indicator of bond strength, with BE < -5 kcal/mol suggesting a stable interaction between TMF and the DEP, and lower BE values reflecting stronger binding affinities [21]. Receptor-ligand interactions were visualized using PyMol 2.5.2 [22].

To validate the docking results, MD simulations were performed using Gromacs 2023. CHARMM 36 force field parameters were applied for the protein [23], while the ligand topology was constructed using GAFF2 force field parameters. The TIP3P water model was employed to solvate the system. Electrostatic interactions were handled using the particle mesh Ewald method and the Verlet algorithm. MD simulations were executed under conditions of constant temperature (300 K) and pressure (1 bar) over 2,500,000 steps, with a step size of 2 fs and a total simulation time of 50 ns. Root mean squared deviation (RMSD) were calculated to assess the stability of complex compounds.

3. Results

3.1. Effect of TMF on protein expression level in HeLa cells

As shown in Fig. 2 and Table 1, treatment of HeLa cells with 50 μM of TMF for 24 h led to the identification of 37 DEPs. Specifically, 17 apoptosis-related proteins were upregulated, including CD40, CD40L, Fas, Fas-L, HSP27, HSP60, IGFBP-1, IGFBP-2, IGF-1sR, Livin, p21, p27, sTNFR2, TRAILR2, TRAILAR3, TRAILR4, and XIAP (Fig. 2A). In the JAK/STAT signaling pathway, EGFR (Ser1070) was downregulated, while Sre (Tyr419), Stat1 (ser727), and Stat2 (Tyr689) were upregulated (Fig. 2B). In the TGFb signaling pathway, ATF2 and c-JUN were downregulated, whereas c-Fos, SMAD1, SMAD2, SMAD4, and SMAD5 were upregulated (Fig. 2C). Within the NFκB signaling pathway, IκBα (S32), MSK1 (S376), NFκB (S536), TAK1 (S412), TBK1 (S172), and ZAP70 (Y292) were upregulated (Fig. 2D). In the MAPK signaling pathway, HSP27 and JNK were downregulated, and MSK2 was upregulated (Fig. 2E), while in the AKT signaling pathway, GSK3A was downregulated (Fig. 2F).

Table 1
Thirty-seven differentially expressed proteins in HeLa cells treated with TMF (50 μM) for 24 h.

Protein	AveExp.E	AveExp.C	logFC	FC (>1.2)	regulation	Entrez ID	Uniport ID
Fas	15.75511	15.43281	0.322298	1.25032	up	355	P25445
CD40	15.56755	15.20546	0.362094	1.28529	up	958	P25942
HSP60	15.20289	14.85137	0.351527	1.275911	up	3329	P10809
CD40L	14.92035	14.57327	0.347079	1.271982	up	959	P29965
p21	14.89228	14.57968	0.312606	1.241949	up	1026	P38936
IGF-1sR	14.44195	13.92932	0.512632	1.426651	up	3479	P05019
IGFBP-2	14.41411	14.0321	0.382004	1.303151	up	3485	P18065
FasL	14.20255	13.89918	0.303369	1.234022	up	356	P48023
p27	14.09551	13.80288	0.292625	1.224867	up	1027	P46527
TRAILR-2	14.03571	13.6818	0.353904	1.278014	up	8795	O14763
sTNF-R2	13.98099	13.65722	0.323763	1.251591	up	7133	P20333
IGFBP-1	13.88088	13.39709	0.483791	1.398413	up	3484	P08833
Livin	13.75238	13.2091	0.543285	1.457287	up	79444	Q96CA5
TRAILR-4	13.67824	13.24379	0.434446	1.351391	up	8793	Q9UBN6
XIAP	13.62999	13.35344	0.276551	1.211295	up	331	P98170
TRAILR-3	13.62021	13.34216	0.278043	1.212549	up	8794	O14798
HSP27	13.53669	13.22952	0.307176	1.237283	up	3315	P04792
IκBα	8.35116	9.186733	0.835573	1.784566	down	4792	P25963
MSK1	8.871351	9.655978	0.784627	1.722647	down	9252	O75582
NFκB	12.08366	12.80398	0.720321	1.647548	down	5970	Q04206
c-Jun	9.157372	9.781032	0.62366	1.540779	down	3725	P05412
ZAP70	11.69695	12.20304	0.506088	1.420194	down	7535	P43403
GSk3a	12.46839	12.94065	0.472255	1.387276	down	2931	P49840
TBK1	10.05922	10.50457	0.445348	1.361643	down	29110	Q9UHD2
ATF2	8.379682	8.81314	0.433458	1.350467	down	1386	P15336
JNK	9.685204	10.07231	0.387102	1.307764	down	5599	P45983
EGFR	8.381586	8.761551	0.379965	1.30131	down	1956	P00535
HSP27	9.799492	10.09028	0.290792	1.223312	down	3315	P04792
TAK1	10.17156	10.45558	0.284019	1.217582	down	6885	O43318
c-Fos	9.039687	8.770829	0.268858	1.204853	up	2353	P01100
SMAD2	7.826231	7.474112	0.352119	1.276434	up	4087	P15796
SRC	10.07318	9.584023	0.489155	1.403622	up	6714	P12931
STAT1	11.23691	10.74147	0.495444	1.409755	up	6772	P42224
SMAD1	8.438251	7.887525	0.550726	1.464823	up	4086	Q15797
SMAD5	10.96276	10.40652	0.556235	1.470427	up	4090	Q99717
STAT2	11.63225	11.07146	0.560783	1.47507	up	6773	P52630
SMAD4	11.34809	10.64773	0.700358	1.624908	up	4089	Q13485

E, experiment; C, control.

3.2. GO functional annotation analysis

A total of 924 BP terms were enriched, including those related to the transmembrane receptor protein serine/threonine kinase signaling pathway, transforming growth factor beta receptor signaling pathway, SMAD protein signal transduction, response to transforming growth factor beta, response to muscle stretch, and response to mechanical stimulus. Notably, the response to mechanical stimulus had the highest number of enriched genes, with 12 genes identified, including NFKBIA, RELA, JUN, MAPK8, EGFR, FOS, FAS, TNFRSF10B, CD40, IGFBP2, SRC, and STAT1. The necroptotic signaling pathway and regulation of cardiac muscle tissue regeneration both exhibited the highest enrichment factor (EF = 172.87), each associated with two genes: FASLG/FAS and CDKN1B/CDKN1A, respectively. Regarding CC, seven GO terms were enriched, including the SMAD protein complex, transcription regulator complex, membrane raft, membrane microdomain, membrane region, RNA polymerase II transcription regulator complex, and nuclear chromatin. Among these, the transcription regulator complex encompassed the highest number of genes, while the SMAD protein complex exhibited the highest enrichment degree (EF = 312.97). For MF, 57 GO terms were identified, such as ubiquitin-like protein ligase binding, ubiquitin protein ligase binding, TRAIL binding, R-SMAD binding, DNA-binding transcription activator activity, RNA polymerase II-specific, DNA-binding transcription activator activity, and DNA-binding transcription factor binding. Ubiquitin-like protein ligase binding was the most significant term (p = 1.69E-14) and included the largest number of genes (13 genes: NFKBIA, RELA, JUN, EGFR, CDKN1A, TNFRSF1B, HSPD1, SMAD2, CD40, SRC, STAT1, SMAD5, STAT2), while TRAIL binding had the highest enrichment degree (EF = 294.93). The top 20 most significant terms, based on adjusted p-value, were visualized and are presented in Fig. 3 and Table 2.

3.3. KEGG pathway enrichment analysis

Based on an adjusted p-value of <0.05, 115 signaling pathways were identified as enriched. The top 20 pathways revealed that the TMF's inhibitory effects on HeLa cells were predominantly associated with the MAPK signaling pathway, TNF signaling pathway, apoptosis, PD-L1 expression and PD-1 checkpoint pathway in cancer, pancreatic cancer, colorectal cancer, NF-kappa B signaling pathway, and FoxO signaling pathway. Of these, the MAPK signaling pathway compassed the highest number of genes, totaling 12 (P = 1.79E-08, EF = 9.93, including RPS6KA5, RELA, JUN, ATF2, MAPK8, EGFR, HSPB1, MAP3K7, FOS, FASLG, FAS, IGF1), while the apoptosis-multiple species pathway had the highest enrichment score (EF = 22.35). These pathways are primarily involved in environmental information processing, cellular processes, organismal systems, and human diseases (Fig. 4B). Pathways with more than six enriched genes were visualized and are presented in Fig. 4A and Table 3.

3.4. PPI analysis for these 37 DEPs

The analysis identified 44 nodes within the network, comprising 37 known and seven predicted DEPs. Analysis of the interactions between nodes revealed that the network had 318 edges, with the number of edges per node in descending order as follows: JUN (36), TP53 (35), FOS (29), MAPK8 (27), XIAP (26), SPC (25), STAT1 (24), RELA (23), CCND1 (21), and CDKN1A (20) (Fig. 5).

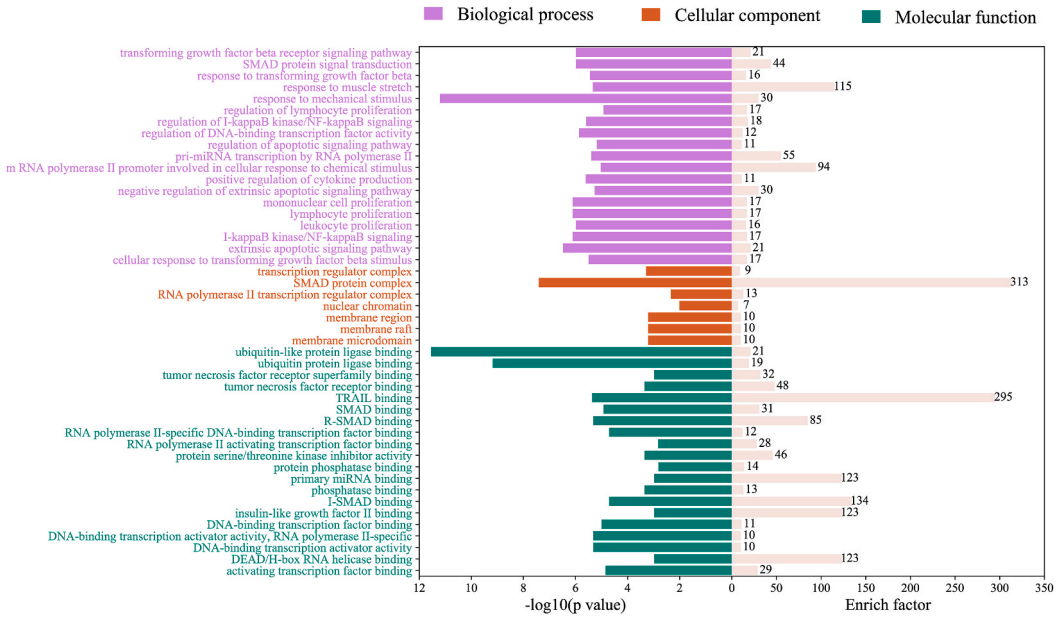

Fig. 3. GO functional annotation for the 37 DEPs, encompassing biological processes, cellular components, and molecular functions.

Table 2
Top 20 most significant GO terms enriched based on the 37 differentially expressed proteins.

GO ID	Description	P. adjust	Gene ID	No	Enrich factor
Biological processes (BP)					
0007178	transmembrane receptor protein serine/threonine kinase signaling pathway	2.67E-06	JUN/MAP3K7/FOS/XIAP/SMAD2/SRC/SMAD1/SMAD5/SMAD4	9	13.37
0007179	transforming growth factor beta receptor signaling pathway	1.05E-06	JUN/MAP3K7/FOS/SMAD2/SRC/SMAD1/SMAD5/SMAD4	8	20.85
0060395	SMAD protein signal transduction	1.05E-06	JUN/FOS/SMAD2/SMAD1/SMAD5/SMAD4	6	44.45
0071559	response to transforming growth factor beta	3.56E-06	JUN/MAP3K7/FOS/SMAD2/SRC/SMAD1/SMAD5/SMAD4	8	16.27
0035994	response to muscle stretch	4.61E-06	NFKBIA/RELA/JUN/FOS	4	115.25
0009612	response to mechanical stimulus	6.24E-12	NFKBIA/RELA/JUN/MAPK8/EGFR/FOS/FAS/TNFRSF10B/CD40/IGFBP2/SRC/STAT1	12	29.63
0050670	regulation of lymphocyte proliferation	1.19E-05	ZAP70/CDKN1A/TNFRSF1B/CD40LG/CD40/IGFBP2/IGF1	7	17.45
0043122	regulation of I-kappaB kinase/NF-kappaB signaling	2.56E-06	RELA/TBK1/HSPB1/MAP3K7/FASLG/TNFRSF10B/CD40/STAT1	8	17.51
0051090	regulation of DNA-binding transcription factor activity	1.38E-06	NFKBIA/RPS6KA5/RELA/JUN/ATF2/MAPK8/MAP3K7/FOS/CD40LG/CD40	10	12.00
2001233	regulation of apoptotic signaling pathway	6.54E-06	RELA/GSK3A/MAPK8/HSPB1/FASLG/FAS/TNFRSF10B/SRC/IGF1	9	11.50
0061614	pri-miRNA transcription by RNA polymerase II	4.07E-06	RELA/JUN/FOS/SMAD1/SMAD4	5	55.17
1901522	positive regulation of transcription from RNA polymerase II promoter involved in cellular response to chemical stimulus	9.24E-06	RELA/SMAD1/SMAD5/SMAD4	4	94.29
0001819	positive regulation of cytokine production	2.46E-06	RELA/TBK1/ATF2/HSPB1/MAP3K7/CD40LG/HSPD1/CD40/SRC/STAT1	10	11.18
2001237	negative regulation of extrinsic apoptotic signaling pathway	5.46E-06	RELA/FASLG/FAS/TNFRSF10B/SRC/IGF1	6	29.92
0032943	mononuclear cell proliferation	7.79E-07	ZAP70/TBK1/CDKN1A/TNFRSF1B/CD40LG/HSPD1/CD40/IGFBP2/IGF1	9	17.03
0046651	lymphocyte proliferation	7.79E-07	ZAP70/TBK1/CDKN1A/TNFRSF1B/CD40LG/HSPD1/CD40/IGFBP2/IGF1	9	17.16
0070661	leukocyte proliferation	1.05E-06	ZAP70/TBK1/CDKN1A/TNFRSF1B/CD40LG/HSPD1/CD40/IGFBP2/IGF1	9	15.66
0007249	I-kappaB kinase/NF-kappaB signaling	7.79E-07	NFKBIA/RELA/TBK1/HSPB1/MAP3K7/FASLG/TNFRSF10B/CD40/STAT1	9	17.35
0097191	extrinsic apoptotic signaling pathway	3.29E-07	RELA/GSK3A/TNFRSF10C/FASLG/FAS/TNFRSF1B/TNFRSF10B/SRC/IGF1	9	20.84
0071560	cellular response to transforming growth factor beta stimulus	3.19E-06	JUN/MAP3K7/FOS/SMAD2/SRC/SMAD1/SMAD5/SMAD4	8	16.66
Cellular components (CC)					
0005667	transcription regulator complex	5.14E-04	RELA/JUN/FOS/SMAD2/SMAD1/SMAD5/SMAD4	7	9.24
0071141	SMAD protein complex	3.91E-08	SMAD2/SMAD1/SMAD5/SMAD4	4	312.97
0090575	RNA polymerase II transcription regulator complex	4.63E-03	JUN/FOS/SMAD2/SMAD4	4	13.20
0000790	nuclear chromatin	9.76E-03	RELA/JUN/SMAD2/STAT1/SMAD4	5	7.28
0098589	membrane region	6.21E-04	ZAP70/EGFR/FASLG/FAS/TNFRSF1B/SRC	6	10.02
0045121	membrane raft	6.21E-04	ZAP70/EGFR/FASLG/FAS/TNFRSF1B/SRC	6	10.43
0098857	membrane microdomain	6.21E-04	ZAP70/EGFR/FASLG/FAS/TNFRSF1B/SRC	6	10.40
Molecular functions (MF)					
0044389	ubiquitin-like protein ligase binding	2.83E-12	NFKBIA/RELA/JUN/EGFR/CDKN1A/TNFRSF1B/HSPD1/SMAD2/CD40/SRC/STAT1/SMAD5/STAT2	13	20.75
0031625	ubiquitin protein ligase binding	6.65E-10	NFKBIA/RELA/JUN/EGFR/CDKN1A/TNFRSF1B/HSPD1/SMAD2/CD40/SRC/SMAD5	11	18.65
0032813	tumor necrosis factor receptor superfamily binding	1.04E-03	FASLG/CD40LG/STAT1	3	32.06
0005164	tumor necrosis factor receptor binding	4.42E-04	FASLG/CD40LG/STAT1	3	47.57

(*continued on next page*)

Table 2 (*continued*)

GO ID	Description	P. adjust	Gene ID	No	Enrich factor
0045569	TRAIL binding	4.32E-06	TNFRSF10C/TNFRSF10B/TNFRSF10D	3	294.93
0046332	SMAD binding	1.18E-05	JUN/FOS/SMAD2/SMAD1/SMAD4	5	30.72
0070412	R-SMAD binding	4.86E-06	JUN/FOS/SMAD2/SMAD4	4	85.49
0061629	RNA polymerase II-specific DNA-binding transcription factor binding	1.93E-05	NFKBIA/RELA/JUN/ATF2/FOS/SRC/STAT1	7	12.42
0001102	RNA polymerase II activating transcription factor binding	1.49E-03	JUN/ATF2/FOS	3	27.82
0030291	protein serine/threonine kinase inhibitor activity	4.42E-04	HSPB1/CDKN1B/CDKN1A	3	46.08
0019903	protein phosphatase binding	1.53E-03	TBK1/EGFR/CDKN1B/STAT1	4	14.04
0070878	primary miRNA binding	1.04E-03	SMAD2/SMAD1	2	122.89
0019902	phosphatase binding	4.42E-04	TBK1/EGFR/CDKN1B/SMAD2/STAT1	5	13.29
0070411	I-SMAD binding	1.93E-05	SMAD2/SMAD1/SMAD4	3	134.06
0031995	insulin-like growth factor II binding	1.04E-03	IGFBP2/IGFBP1	2	122.89
0140297	DNA-binding transcription factor binding	9.89E-06	NFKBIA/RELA/JUN/ATF2/FOS/SMAD2/SRC/STAT1	8	11.20
0001228	DNA-binding transcription activator activity, RNA polymerase II-specific	4.86E-06	RELA/JUN/ATF2/FOS/SMAD2/STAT1/SMAD1/STAT2/SMAD4	9	10.08
0001216	DNA-binding transcription activator activity	4.86E-06	RELA/JUN/ATF2/FOS/SMAD2/STAT1/SMAD1/STAT2/SMAD4	9	10.05
0017151	DEAD/H-box RNA helicase binding	1.04E-03	SMAD1/SMAD5	2	122.89
0033613	activating transcription factor binding	1.42E-05	RELA/JUN/ATF2/FOS/SMAD2	5	28.92

3.5. Molecular docking and molecular dynamics simulation

Following the PPI analysis, molecular docking was conducted to evaluate the binding strength between TMF and these 44 nodes. Using AGFR software (Version 1.2) for active site prediction, the optimal docking sites were determined based on the docking scores. The results indicated that 23 of the 44 proteins exhibited BE of less than 0 kcal/mol with TMF (Table 4), including CDKN1B, SMAD4, NFKBIA, SMAD5, XIAP, ZAP70, IRF3, CD40, HSPB1, FAS, TBK1, BCAR1, IGFBP2, FASLG, CDKN1A, BIRC7, TNFRSF10C, CCND1, JUN, GSK3A, STAT1, MAPK9, and TNFRSF1B. Among these 23 proteins, only MAPK9 and TNFRSF1B had BEs greater than −5 kcal/mol (Fig. 6G). The interactions of six proteins with the strongest binding affinities to TMF are illustrated in Fig. 6A–F.

To validate the molecular docking results, two proteins including CDKN1B and SMAD5 were selected for molecular dynamics simulation. The findings indicated that both the TMF-CDKN1B and TMF-SMAD5 complexes achieved equilibrium after 50 ns, with RMSD values of 2.07 ± 0.23 Å and 2.46 ± 0.34 Å, respectively, suggesting high stability for both two complexes, with TMF-CDKN1B exhibiting greater stability than TMF-SMAD5 (Fig. 7A). The radius of gyration (Rg) analysis further confirmed the stability of both complexes throughout the simulation (Fig. 7B). Additionally, the fluctuation range of solvent-accessible surface area (SASA) values indicated that TMF binding to CDKN1B and SMAD5 did not induce significant conformational changes (Fig. 7C). Moreover, the root mean square fluctuation (RMSF) values for both complexes were relatively low, ranging from 1 to 4 Å except for the C-terminal region, with the TMF-SMAD5 complex displaying greater flexibility compared to TMF-CDKN1B (Fig. 7D and E). In summary, these results suggest that TMF likely exerts its effects by directly interacting with these two proteins, supporting the reliability of the molecular docking result.

4. Discussion

TMF, a potent bioflavonoid belonging to the PMF family, is predominantly found in *Citrus* plants. Sytrinol, a U.S.-patented food supplement rich in citrus PMFs, is widely utilized globally for the prevention of cardiovascular and cerebrovascular diseases. PMFs have gained significant attention for their medicinal potential, becoming a major focus of research in recent years. However, compared to nobiletin and tangeretin—the two most extensively studied citrus PMFs—TMF has received relatively little attention. This discrepancy may be attributed to the lower concentrations of TMF in Citrus plants, which has historically hindered its availability for research. To address this issue, our previous study [16] successfully overcame the challenge of TMF availability through a semi-synthetic method, demonstrating for the first time that TMF exhibited greater potency in inhibiting HeLa cell growth than nobiletin and tangeretin, and establishing its pharmacokinetic parameters in rats, thereby positioning TMF as a promising therapeutic

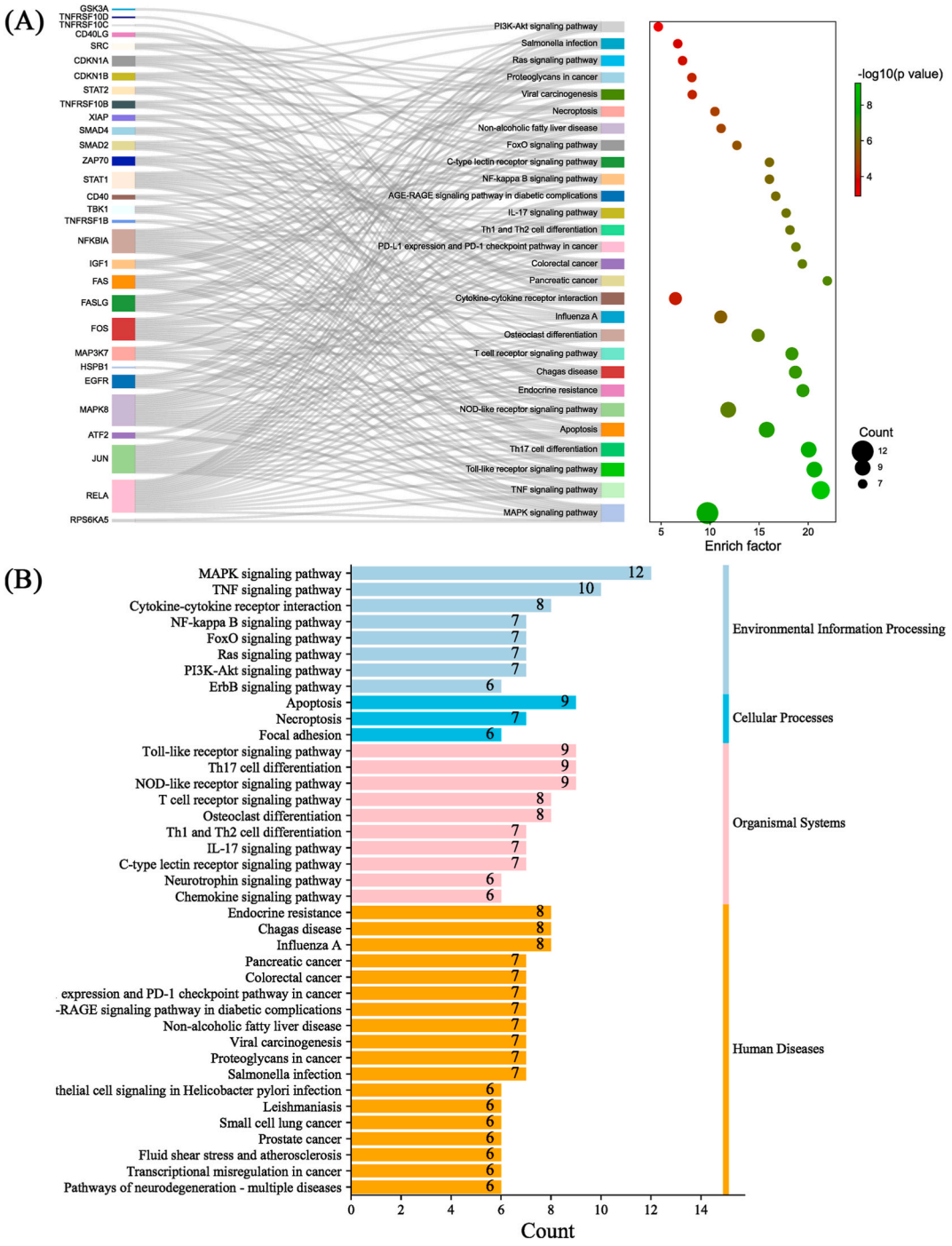

Fig. 4. (A) KEGG pathway enrichment analysis of the 37 DEPs, and (B) KEGG classification of these pathways.

candidate for CCA treatment. This makes it imperative to further elucidate the mechanisms by which TMF exerts its effects against HeLa cancer cells.

In the present study, antibody arrays were employed to assess the proteomic profiles of HeLa cells following TMF treatment. The analysis revealed the upregulation of 17 apoptosis-related proteins, including p21, p27, Fas, and FasL. Both p21 and p27 are critical members of the CIP/KIP family of cyclin-dependent kinase inhibitors, with numerous studies indicating that their expression levels are inversely correlated with cancer invasion and recurrence [24]. The upregulation of these proteins can inhibit CCA cell division and proliferation while promoting differentiation and apoptosis [25–27]. Additionally, whereas Fas and FasL, two pro-apoptotic proteins are known to significantly induce apoptosis in HeLa cells when activated [28,29]. Among the 55 identified phosphorylation sites,

Table 3
KEGG signaling pathway enrichment for the 37 differentially expressed proteins.

ID	Signaling pathway	p.adjust	geneID	Count	Enrich factor
hsa04010	MAPK	1.79E-08	RPS6KA5/RELA/JUN/ATF2/MAPK8/EGFR/HSPB1/MAP3K7/FOS/FASLG/FAS/IGF1	12	9.73
hsa04668	TNF	5.94E-10	NFKBIA/RPS6KA5/RELA/JUN/ATF2/MAPK8/MAP3K7/FOS/FAS/TNFRSF1B	10	21.28
hsa04620	Toll-like receptor	6.75E-09	NFKBIA/RELA/JUN/TBK1/MAPK8/MAP3K7/FOS/CD40/STAT1	9	20.63
hsa04659	Th17 cell differentiation	7.64E-09	NFKBIA/RELA/JUN/ZAP70/MAPK8/FOS/SMAD2/STAT1/SMAD4	9	20.05
hsa04210	Apoptosis	4.01E-08	NFKBIA/RELA/JUN/MAPK8/FOS/XIAP/FASLG/FAS/TNFRSF10B	9	15.78
hsa04621	NOD-like receptor	2.82E-07	NFKBIA/RELA/JUN/TBK1/MAPK8/MAP3K7/XIAP/STAT1/STAT2	9	11.85
hsa01522	Endocrine resistance	5.31E-08	JUN/MAPK8/EGFR/FOS/CDKN1B/CDKN1A/SRC/IGF1	8	19.46
hsa05142	Chagas disease	6.88E-08	NFKBIA/RELA/JUN/MAPK8/FOS/FASLG/FAS/SMAD2	8	18.70
hsa04660	T cell receptor	7.59E-08	NFKBIA/RELA/JUN/ZAP70/MAPK8/MAP3K7/FOS/CD40LG	8	18.34
hsa04380	Osteoclast differentiation	2.83E-07	NFKBIA/RELA/JUN/MAPK8/MAP3K7/FOS/STAT1/STAT2	8	14.90
hsa05164	Influenza A	2.00E-06	NFKBIA/RELA/TBK1/FASLG/FAS/TNFRSF10B/STAT1/STAT2	8	11.09
hsa04060	Cytokine-cytokine receptor interaction	7.43E-05	TNFRSF10C/FASLG/FAS/TNFRSF1B/CD40LG/TNFRSF10B/CD40/TNFRSF10D	8	6.46
hsa05212	Pancreatic cancer	1.76E-07	RELA/MAPK8/EGFR/CDKN1A/SMAD2/STAT1/SMAD4	7	21.96
hsa05210	Colorectal cancer	3.43E-07	JUN/MAPK8/EGFR/FOS/CDKN1A/SMAD2/SMAD4	7	19.40
hsa05235	PD-L1 expression and PD-1 checkpoint pathway in cancer	4.20E-07	NFKBIA/RELA/JUN/ZAP70/EGFR/FOS/STAT1	7	18.75
hsa04658	Th1 and Th2 cell differentiation	5.11E-07	NFKBIA/RELA/JUN/ZAP70/MAPK8/FOS/STAT1	7	18.14
hsa04657	IL-17	5.73E-07	NFKBIA/RELA/JUN/TBK1/MAPK8/MAP3K7/FOS	7	17.75
hsa04933	AGE-RAGE in diabetic complications	8.51E-07	RELA/JUN/MAPK8/CDKN1B/SMAD2/STAT1/SMAD4	7	16.69
hsa04064	NF-kappa B	1.05E-06	NFKBIA/RELA/ZAP70/MAP3K7/XIAP/CD40LG/CD40	7	16.04
hsa04625	C-type lectin receptor	1.05E-06	NFKBIA/RELA/JUN/MAPK8/SRC/STAT1/STAT2	7	16.04
hsa04068	FoxO	4.39E-06	MAPK8/EGFR/CDKN1B/FASLG/CDKN1A/IGF1/SMAD4	7	12.74
hsa04932	Non-alcoholic fatty liver disease	1.01E-05	RELA/JUN/GSK3A/MAPK8/FOS/FASLG/FAS	7	11.12
hsa04217	Necroptosis	1.42E-05	MAPK8/XIAP/FASLG/FAS/TNFRSF10B/STAT1/STAT2	7	10.49
hsa05203	Viral carcinogenesis	6.17E-05	NFKBIA/RELA/JUN/ATF2/CDKN1B/CDKN1A/SRC	7	8.18
hsa05205	Proteoglycans in cancer	6.25E-05	EGFR/FASLG/CDKN1A/FAS/SMAD2/SRC/IGF1	7	8.14
hsa04014	Ras	1.30E-04	RELA/ZAP70/TBK1/MAPK8/EGFR/FASLG/IGF1	7	7.19
hsa05132	Salmonella infection	2.00E-04	NFKBIA/RELA/JUN/MAPK8/MAP3K7/FOS/TNFRSF10B	7	6.70
hsa04151	PI3K-Akt	1.26E-03	RELA/ATF2/EGFR/CDKN1B/FASLG/CDKN1A/IGF1	7	4.71
hsa05120	Epithelial cell signaling in Helicobacter pylori infection	1.93E-06	NFKBIA/RELA/JUN/MAPK8/EGFR/SRC	6	20.43
hsa05140	Leishmaniasis	3.23E-06	NFKBIA/RELA/JUN/MAP3K7/FOS/STAT1	6	18.58
hsa04012	ErbB signaling pathway	5.51E-06	JUN/MAPK8/EGFR/CDKN1B/CDKN1A/SRC	6	16.83
hsa05222	Small cell lung cancer	8.58E-06	NFKBIA/RELA/XIAP/CDKN1B/CDKN1A/BIRC7	6	15.55
hsa05215	Prostate cancer	1.11E-05	NFKBIA/RELA/EGFR/CDKN1B/CDKN1A/IGF1	6	14.75
hsa04722	Neurotrophin signaling pathway	3.34E-05	NFKBIA/RPS6KA5/RELA/JUN/MAPK8/FASLG	6	12.02
hsa05418	Fluid shear stress and atherosclerosis	7.04E-05	RELA/JUN/MAPK8/MAP3K7/FOS/SRC	6	10.29
hsa04062	Chemokine signaling pathway	0.000367	NFKBIA/RELA/GSK3A/SRC/STAT1/STAT2	6	7.45
hsa05202	Transcriptional misregulation in cancer	0.000367	RELA/CDKN1B/CDKN1A/CD40/IGF1/SMAD1	6	7.45
hsa04510	Focal adhesion	0.00045	JUN/MAPK8/EGFR/XIAP/SRC/IGF1	6	7.12
hsa05022	Pathways of neurodegeneration - multiple diseases	0.021689	RELA/TBK1/MAPK8/FASLG/FAS/TNFRSF1B	6	3.01

several key proteins were affected by TMF treatment. EGFR (Ser1070), ATF2, c-JUN, GSK3A, HSP27, and JNK were downregulated, whereas Sre (Tyr419), Stat1 (Ser727), Stat2 (Tyr689), c-Fos, SMAD1, SMAD2, SMAD4, SMAD5, IκBα (S32), MSK1(S376), NF-κB (S536), TAK1 (S412), TBK1 (S172), ZAP70 (Y292), and MSK2 were upregulated. EGFR, a member of the HER family, is closely associated with tumor development and progression, with clinical trials showing significantly higher EGFR expression levels in CCA tissues compared to adjacent tissues [30,31]. EGFR has been established as an effective target for cancer treatment, and inhibitors such as gefitinib, erlotinib, and osimertinib are frequently prescribed to patients with cancers [32]. The findings from the phosphorylated antibody array suggest that TMF can suppress EGFR activation, mirroring the action mechanism of these EGFR inhibitors.

GO functional annotation of the 37 DEPs revealed that TMF significantly impacted various functions in HeLa cancer cells, including the positive regulation of transcription from the RNA polymerase II promoter in response to chemical stimuli, SMAD protein complex formation, and TRAKL binding. Notably, the SMAD protein complex—a core GO term—was further substantiated by PPI analysis and molecular docking, with SMAD4 and SMAD5 exhibiting lower BE with TMF. As key signal transduction molecules downstream of the transforming growth factor β (TGF-β) receptor family, SMAD proteins, particularly SMAD2/3, are crucial in transmitting TGF-β signals from cell-surface receptors to the nucleus [33]. TGF-β itself has been implicated in the formation, invasion, progression, metastasis,

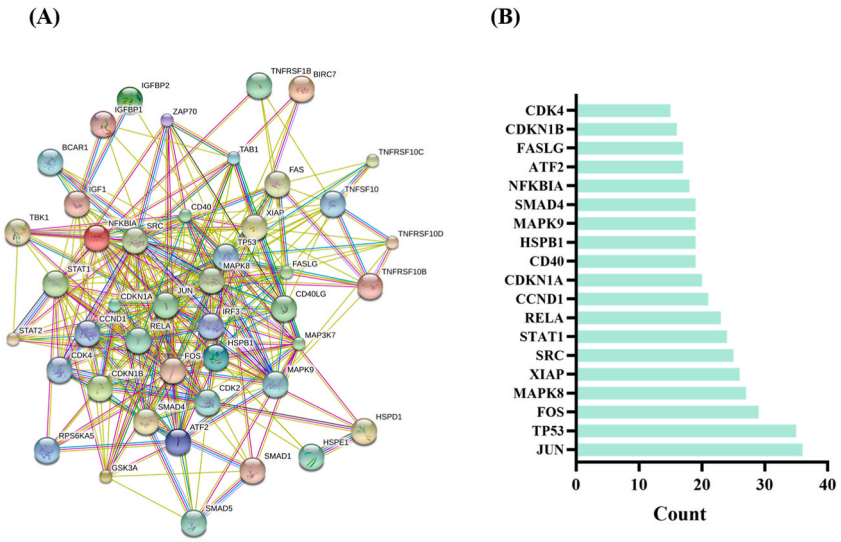

Fig. 5. (A) Protein-protein interaction network of the 37 DEPs, and (B) graphic representation of the degree of connectivity for the top 19 DEPs.

Table 4
Docking parameters of TMF with target proteins.

No	Targets	PDB ID	Binding energy (kcal/mol)	No	Targets	PDB ID	Binding energy (kcal/mol)
1	JUN	1JNM	−5.1	23	IGFBP1	1ZT3	0
2	BIRC7	1OXN	−5.6	24	IRF3	1J2F	−6.7
3	IGFBP2	2H7T	−5.9	25	MAP3K7	4GS6	0
4	RELA	3RC0	0	26	MAPK8	3ELJ	0
5	ATF2	4H36	0	27	MAPK9	3E7O	−4.5
6	BCAR1	1WYX	−5.9	28	NFκBIA	1NFN	−6.9
7	CCND1	2W96	−5.4	29	RPS6KA5	3KN6	0
8	CD40	1LB6	−6.6	30	SMAD1	1KHU	0
9	CD40LG	1ALY	0	31	SMAD4	1YGS	−7.4
10	CDK2	1AQ1	0	32	SMAD5	6FZS	−6.9
11	CDK3	7XQK	0	33	SRC	1A07	0
12	CDKN1A	2ZVV	−5.7	34	STAT1	3WWT	−5.0
13	CDKN1B	1H27	−8.0	35	STAT2	6UX2	0
14	FAS	3TJE	−5.9	36	TAB1	2J4O	0
15	FASLG	5L19	−5.9	37	TBK1	4IM0	−5.9
16	FOS	1A02	0	38	TNFRSF1B	1CA9	−1.5
17	GSK3A	7SXF	−5.1	39	TNFRSF10B	1D0G	0
18	HSPB1	3Q9B	−6.1	40	TNFSF10	1D4V	0
19	HSPD1	4PJ1	0	41	TP53	1AIE	0
20	HSPE1	6HT7	0	42	XIAP	1NW9	−6.8
21	IGF1	2DSP	0	43	ZAP70	5O76	−6.8
22	TNFRSF10D	AF-Q9UBN6	0	44	TNFRSF10C	AF-Q05D7	−5.5

and treatment of CCA [34]. Proteomics results showed that SMAD1, SMAD2, SMAD4, and SMAD5 were upregulated, with SMAD2 expression notably reduced in CCA [35]. This study suggests that the TGF-β/SMAD2 signaling pathway may play a significant role in the anti-CCA efficacy of TMF. Further KEGG pathway enrichment analysis indicated that TMF primarily affects the MAPK, TNF, and apoptosis signaling pathways. Similar PMFs, such as tangeretin, sudachitin, and nobiletin, have also demonstrated inhibitory effects on tumor cells through the MAPK signaling pathway [36–38]. Molecular docking results revealed that TMF binds effectively to 21 targets, with BEs below −5 kcal/mol. Despite identifying 10 core nodes *via* PPI analysis, only half showed direct binding with TMF, suggesting that TMF may influence some targets indirectly by acting on upstream signaling molecules rather than directly interacting with them. Subsequent MD simulations confirmed that TMF directly on targets these proteins. These findings underscore that TMF's efficacy against HeLa cells is achieved through its multi-target, multi-pathway, and multi-functional mechanisms.

In our previous study, four permethylated tetramethoxyflavones were evaluated for their anti-cancer bioactivity: 5,6,7,4′-tetramethoxyflavone (TMF), 5,7,3′,4′- tetramethoxyflavone, 3,7,3′,4′-tetramethoxyflavone and 3,5,7,4′-tetramethoxyflavone. Among these, only TMF exhibited strong inhibitory effects against HeLa cancer cells, while the other three compounds showed no significant inhibition of HeLa, A549, HepG2, and HCT116 cancer cells (IC_{50} > 100 μM). Despite their lack of efficacy in cancer suppression, the other three PMFs demonstrated substantial biological activity in other areas. For instance, 5,7,3′,4′-tetramethoxyflavone significantly inhibited the expression of α-glucosidase [39] and iNOS [40] *in vitro* and has shown therapeutic potential in treating inflammatory

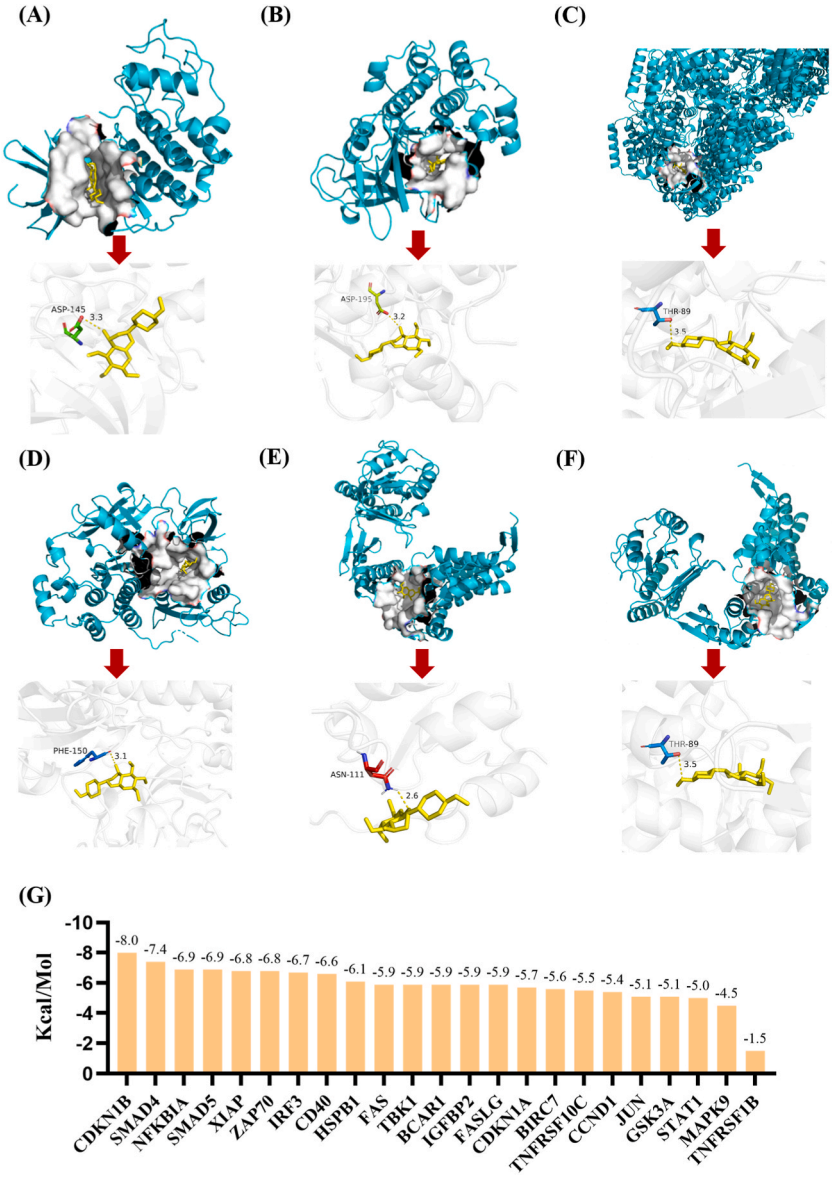

Fig. 6. Molecular docking analysis of TMF with the 44 node proteins. Interactions between TMF and the top six proteins: (A) CDKN1B, (B) SMAD4, (C) NFKBIA, (D) SMAD5, (E) XIAP, and (F) ZAP70. (G) Graphic representation of the proteins with binding energies less than 0 kcal/Mol.

diseases by inhibiting neuropeptide-stimulated proinflammatory mediator release *via* mTOR activation [41], as well as by suppressing miR-29a/Wnt/β-catenin signaling through the upregulation of Foxo3a activity [42]. Similarly, 3,7,3′,4′-tetramethoxyflavone was found to suppress inflammation by reducing NO production [43], while 3,5,7,4′-tetramethoxyflavone exhibited potential in preventing cataracts by inhibiting MMP9 and MAPKs [44]. Although these four compounds share the same number of methoxy group and have highly similar chemical structures, their mechanisms of action and biological targets differ significantly.

5. Conclusion

This study suggests that the inhibitory effects of TMF against HeLa cancer were primarily mediated through the MAPK, TNF, and apoptosis signaling pathways. These findings provide a foundation for further exploration of TMF's medicinal potential against HeLa cancer. However, this study assessed the effect of TMF on HeLa cell proteomics only at the cellular level *in vitro*, with the current findings primarily derived from in silico bioinformatics and molecular docking analyses. To strengthen the reliability of these results, additional research is needed using animal models, along with transcriptomics, proteomics western blotting, and qPCR experiments.

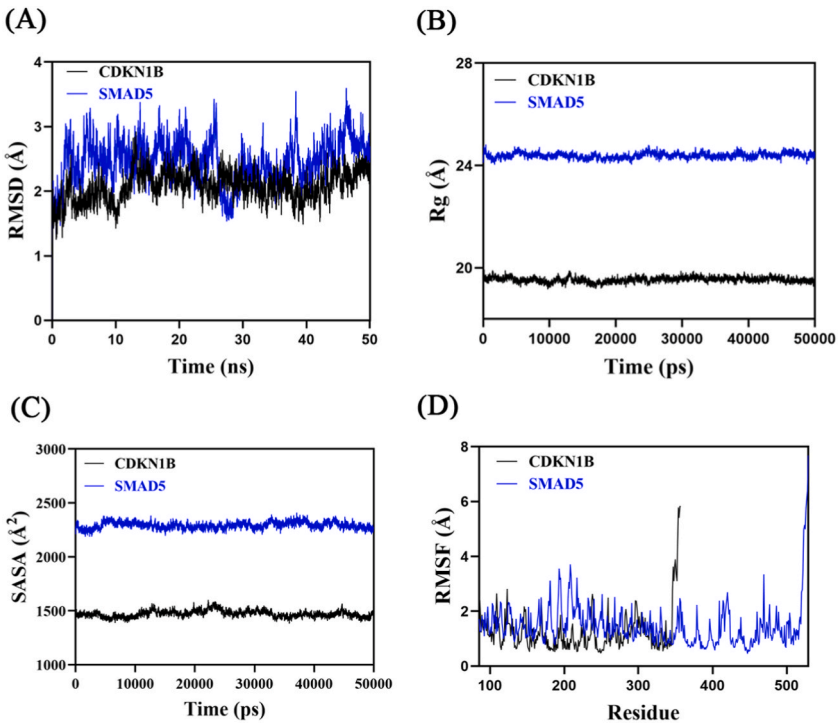

Fig. 7. Molecular dynamics simulation of TMF-CDKN1B and TMF-SMAD5 complexes. (A) RMSD values of the two complexes over time, (B) Rg values of the two complexes, (C) SASA values of the two complexes, (D) RMSF values of amino acid backbone atoms in TMF-CDKN1B, and (E) RMSF values of amino acid backbone atoms in TMF-SMAD5.

Funding

This work was supported by the Natural Science Foundation of Hainan Province (No. 823MS148), China; the Foundation of Hainan Health Committee (No. 22A200257), China; and the Foundation of Hainan Educational Committee (No. Hnky2023-25), China.

Ethics declarations

Not applicable.

Consent for publication

Not applicable.

Data availability statement

The authors confirm that all data supporting the findings of this study are included in the article.

CRediT authorship contribution statement

Qiang You: Writing – original draft, Funding acquisition, Conceptualization. **Lan Li:** Writing – review & editing, Writing – original draft. **Haiyan Ding:** Visualization, Formal analysis. **Youping Liu:** Writing – review & editing, Supervision.

Declaration of competing interest

The authors declare that they have no known competing financial interests or personal relationships that could have appeared to influence the work reported in this paper.

References

[1] World Health Organization (WHO), Cancer Fact Sheets, 2020 gco.iarc.fr/today/data/factsheets/cancers/23-cervix-uteri-fact-sheet.pdf[Z]//.

[2] P. Olusola, H.N. Banerjee, J.V. Philley, S. Dasgupta, Human papilloma virus-associated cervical cancer and health disparities, Cells-Basel 8 (6) (2019) 622–633.
[3] P.A. Cohen, A. Jhingran, A. Oaknin, L. Denny, Cervical cancer, Lancet 393 (10167) (2019) 169–182.
[4] A. Duenas-Gonzalez, J.J. Zarba, F. Patel, J.C. Alcedo, S. Beslija, L. Casanova, P. Pattaranutaporn, S. Hameed, J.M. Blair, H. Barraclough, M. Orlando, Phase iii, open-label, randomized study comparing concurrent gemcitabine plus cisplatin and radiation followed by adjuvant gemcitabine and cisplatin versus concurrent cisplatin and radiation in patients with stage iib to iva carcinoma of the cervix, J. Clin. Oncol. 29 (13) (2011) 1678–1685.
[5] A. Rayan, J. Raiyn, M. Falah, Nature is the best source of anticancer drugs: indexing natural products for their anticancer bioactivity, PLoS One 12 (11) (2017) 1–12.
[6] D.J. Newman, G.M. Cragg, Natural products as sources of new drugs over the 30 years from 1981 to 2010, J. Nat. Prod. 75 (3) (2012) 311–335.
[7] Z. Peng, H. Zhang, W. Li, Z. Yuan, Z. Xie, H. Zhang, Y. Cheng, J. Chen, J. Xu, Comparative profiling and natural variation of polymethoxylated flavones in various citrus germplasms, Food Chem. 354 (2021) 129499.
[8] C. Tran, M.D. Tri, N. Tien-Trung, N. Phan, C.D. Phan, T. Tran, T. Do, N. Tran, T. Tran, T. Duong, Nervione, a new benzofuran derivative from *nervilia concolor*, Nat. Prod. Res. 36 (20) (2022) 5148–5154.
[9] R. Alkhatib, S. Joha, M. Cheok, V. Roumy, T. Idziorek, C. Preudhomme, B. Quesnel, S. Sahpaz, F. Bailleul, T. Hennebelle, Activity of ladanein on leukemia cell lines and its occurrence in *marrubium vulgare*, Planta Med. 76 (1) (2010) 86–87.
[10] Y. Chan, C. Wang, T. Hwang, S. Juang, H. Hung, P. Kuo, P. Chen, T. Wu, The constituents of the stems of *cissus assamica* and their bioactivities, Molecules 23 (11) (2018) 2791–2799.
[11] W. Chen, Y. Zhao, W. Sun, Y. He, Y. Liu, Q. Jin, X. Yang, X. Luo, "kidney tea" and its bioactive secondary metabolites for treatment of gout, J. Agr. Food Chem. 68 (34) (2020) 9131–9138.
[12] C. Cheng, Q. Shou, J. Lang, L. Jin, X. Liu, D. Tang, Z. Yang, H. Fu, Gehua jiecheng decoction inhibits diethylnitrosamine-induced hepatocellular carcinoma in mice by improving tumor immunosuppression microenvironment, Front. Pharmacol. 11 (2020) 809.
[13] J.A. Manthey, N. Guthrie, Antiproliferative activities of citrus flavonoids against six human cancer cell lines, J. Agr. Food Chem. 50 (21) (2002) 5837–5843.
[14] H. Ohtani, T. Ikegawa, Y. Honda, N. Kohyama, S. Morimoto, Y. Shoyama, M. Juichi, M. Naito, T. Tsuruo, Y. Sawada, Effects of various methoxyflavones on vincristine uptake and multidrug resistance to vincristine in p-gp-overexpressing k562/adm cells, Pharm. Res.-Dordr 24 (10) (2007) 1936–1943.
[15] C.V. Pereira, M. Duarte, P. Silva, A.B. Da Silva, C.M.M. Duarte, A. Cifuentes, V. Garcia-Canas, M.R. Bronze, C. Albuquerque, A.T. Serra, Polymethoxylated flavones target cancer stemness and improve the antiproliferative effect of 5-fluorouracil in a 3d cell model of colorectal cancer, Nutrients 11 (326) (2019) 1–20.
[16] Q. You, D. Li, H. Ding, H. Chen, Y. Hu, Y. Liu, Pharmacokinetics and metabolites of 12 bioactive polymethoxyflavones in rat plasma, J. Agr. Food Chem. 69 (43) (2021) 12705–12716.
[17] X. Liu, P. Zhang, Y. Song, Z. Xu, L. Song, Antibody microarrays technology and applications in cancer research, Chin. J. Dis. Control Prev. 10 (2) (2006) 189–192.
[18] H. Li, F. Chen, J. Wang, Y. Tian, Y. Wang, H. Wang, C. Chen, Target screening for baicalin induced apoptosis in human gastric cancer sgc-7901 cells based on apoptosis antibody array, Tradit. Chin. Drug Res. Clin. Pharmacol. 29 (5) (2018) 540–545.
[19] X. Teng, J. Zhang, Y. Shi, Y. Liu, Y. Yang, J. He, S. Luo, Y. Huang, Y. Liu, D. Liu, Y. Li, S. Zhang, R.P. Huang, D. Wang, J. Xu, Comprehensive profiling of inflammatory factors revealed that growth differentiation factor-15 is an indicator of disease severity in covid-19 patients, Front. Immunol. 12 (2021) 662465.
[20] S. Maere, K. Heymans, M. Kuiper Bingo, A cytoscape plugin to assess overrepresentation of gene ontology categories in biological networks, Bioinformatics 21 (16) (2005) 3448–3449.
[21] S. Tao, J. Li, H. Wang, S. Ding, W. Han, R. He, Z. Ren, G. Wei, Anti-colon cancer effects of *dendrobium officinale* kimura & migo revealed by network pharmacology integrated with molecular docking and metabolomics studies, Front. Med. 9 (2022) 879986.
[22] A.C. Egil, B. Ozdemir, B. Gok, S. Kecel-Gunduz, Y. Budama-Kilinc, Synthesis, characterization, biological activities and molecular docking of *epilobium parviflorum* aqueous extract loaded chitosan nanoparticles, Int. J. Biol. Macromol. 161 (2020) 947–957.
[23] S. Jo, T. Kim, V.G. Iyer, W. Im, Charmm-gui: a web-based graphical user interface for charmm, J. Comput. Chem. 29 (11) (2008) 1859–1865.
[24] M. Jiang, K. Shu, Research progress on the expression of p21 and p27 proteins in tumors, Practical Clinical Medicine 19 (6) (2018), 101-103, 107.
[25] Q. Guo, Y. Xiong, Y. Song, K. Hua, S. Gao, Arhgap17 suppresses tumor progression and up-regulates p21 and p27 expression via inhibiting pi3k/akt signaling pathway in cervical cancer, Gene 692 (2019) 9–16.
[26] Y.H. Chen, J.X. Wu, S.F. Yang, M.L. Chen, T.H. Chen, Y.H. Hsiao, Metformin potentiates the anticancer effect of everolimus on cervical cancer in vitro and in vivo, Cancers 13 (18) (2021) 4612–4635.
[27] M.H. Wu, C.L. Lin, H.L. Chiou, S.F. Yang, C.Y. Lin, C.J. Liu, Y.H. Hsieh, Praeruptorin a inhibits human cervical cancer cell growth and invasion by suppressing mmp-2 expression and erk1/2 signaling, Int. J. Mol. Sci. 19 (1) (2017) 10–22.
[28] Y. Peng, C. Guo, Y. Yang, F. Li, Y. Zhang, B. Jiang, Q. Li, Baicalein induces apoptosis of human cervical cancer hela cells in vitro, Mol. Med. Rep. 11 (3) (2015) 2129–2134.
[29] X. Zhu, J. Wang, Y. Ou, W. Han, H. Li, Polyphenol extract of *phyllanthus emblica* (peep) induces inhibition of cell proliferation and triggers apoptosis in cervical cancer cells, Eur. J. Med. Res. 18 (1) (2013) 46–50.
[30] R. Maisaidi, J. Sha, L. Han, Study on the expression and significance of egfr in cervical cancer, Journal of Bingtuan Medicine 20 (2) (2022) 34–36.
[31] S. Muthusami, R. Sabanayagam, L. Periyasamy, B. Muruganantham, W.Y. Park, A review on the role of epidermal growth factor signaling in the development, progression and treatment of cervical cancer, Int. J. Biol. Macromol. 194 (2022) 179–187.
[32] C.R. Chong, P.A. Janne, The quest to overcome resistance to egfr-targeted therapies in cancer, Nat. Med. 19 (11) (2013) 1389–1400.
[33] X.H. Feng, R. Derynck, Specificity and versatility in tgf-beta signaling through smads, Annu. Rev. Cell Dev. Biol. 21 (2005) 659–693.
[34] H. Zhu, H. Luo, Z. Shen, X. Hu, L. Sun, X. Zhu, Transforming growth factor-beta1 in carcinogenesis, progression, and therapy in cervical cancer, Tumour Biol 37 (6) (2016) 7075–7083.
[35] K.D. Ki, S.Y. Tong, C.Y. Huh, J.M. Lee, S.K. Lee, S.G. Chi, Expression and mutational analysis of tgf-beta/smads signaling in human cervical cancers, J. Gynecol Oncol 20 (2) (2009) 117–121.
[36] S. Abe, K. Yuasa Sudachitin, A polymethoxyflavone from citrus sudachi, induces apoptosis via the regulation of mapk pathways in human keratinocyte hacat cells, Biochem. Bioph. Res. Co. 519 (2) (2019) 344–350.
[37] W. Raza, S. Luqman, A. Meena, Prospects of tangeretin as a modulator of cancer targets/pathways, Pharmacol. Res. 161 (2020) 105202.
[38] J.H. Yen, C.Y. Lin, C.H. Chuang, H.K. Chin, M.J. Wu, P.Y. Chen, Nobiletin promotes megakaryocytic differentiation through the mapk/erk-dependent egr1 expression and exerts anti-leukemic effects in human chronic myeloid leukemia (cml) k562 cells, Cells-Basel 9 (4) (2020) 877–895.
[39] T. Azuma, S.I. Kayano, Y. Matsumura, Y. Konishi, Y. Tanaka, H. Kikuzaki, Antimutagenic and α-glucosidase inhibitory effects of constituents from *kaempferia parviflora*, Food Chem. 125 (2) (2011) 471–475.
[40] C. Sae-Wong, H. Matsuda, S. Tewtrakul, P. Tansakul, S. Nakamura, Y. Nomura, M. Yoshikawa, Suppressive effects of methoxyflavonoids isolated from *kaempferia parviflora* on inducible nitric oxide synthase (inos) expression in raw 264.7 cells, J. Ethnopharmacol. 136 (3) (2011) 488–495.
[41] A.B. Patel, T.C. Theoharides, Methoxyluteolin inhibits neuropeptide-stimulated proinflammatory mediator release via mtor activation from human mast cells, J. Pharmacol. Exp. Ther. 361 (3) (2017) 462–471.
[42] X. Huang, Z. Chen, W. Shi, R. Zhang, L. Li, H. Liu, L. Wu, Tmf inhibits mir-29a/wnt/β-catenin signaling through upregulating foxo3a activity in osteoarthritis chondrocytes, Drug Des. Dev. Ther. 13 (2019) 2009–2019.
[43] R. Wen, H. Lv, Y. Jiang, P. Tu, Anti-inflammatory flavone and chalcone derivatives from the roots of *pongamia pinnata* (l.) Pierre, Phytochemistry (Elsevier 149 (2018) 56–63.
[44] Y. Miyata, J. Tatsuzaki, J. Yang, H. Kosano, Potential therapeutic agents, polymethoxylated flavones isolated from *kaempferia parviflora* for cataract prevention through inhibition of matrix metalloproteinase-9 in lens epithelial cells, Biol. Pharm. Bull. 42 (10) (2019) 1658–1664.